Focused cylindrical vector beam assisted microscopic pSPR biosensor with an ultra wide dynamic range

Rong Wang,[1,†] Chonglei Zhang,[1,†] Yong Yang,[1,3] Siwei Zhu,[2] and X.-C. Yuan[1,4]

[1]*Institute of Modern Optics, Key Laboratory of Optoelectronic Information Science & Technology, Ministry of Education of China, Nankai University, Tianjin, China, 300071*

[2]*Nankai University Affiliated Hospital, Tianjin, China, 300121*

[3]*e-mail: yangyong@nankai.edu.cn*

[4]*e-mail: xcyuan@nankai.edu.cn*

Received December 13, 2011; revised February 21, 2012; accepted April 11, 2012; posted April 12, 2012 (Doc. ID 159906); published May 30, 2012

A novel phase-sensitive surface plasmon resonance (pSPR) biosensor based on differential phase measurement between two cylindrical vector beams, namely radially polarized and azmuthally polarized beams, is proposed and studied in an inverted microscope. Different from a fixed angle or a relatively small angular range for SPR excitation in the attenuated total reflection (ATR) configuration, the signal beam focused by a total internal reflection fluorescence microscopic objective contains the entire angular range from 0 to the maximum angle given by the numerical aperture, leading to a dynamic range of 0.41 RIU which is over seven times wider than the best result of the ATR pSPR sensor. Moreover, with the technique of differential phase measurement between radial and azimuthal polarizations employed in our configuration, high sensitivity of $\pm 9.05 \times 10^{-8}$ refractive index unit/1 deg can simultaneously be achieved in principle. The proposed technique maintains the unique advantages in terms of securing high imaging resolution and sensitivity with an ultra-wide dynamic range simultaneously.

OCIS codes: 170.3890, 120.5060, 240.6680, 120.3180, 180.4243.

Surface plasmons (SPs) have gathered considerable amount of interest for sensing applications because they are very sensitive to variations of surrounding media. In optical sensing, surface plasmon resonance (SPR) biosensors have increasingly been exploited in the last two decades as an important tool for the study of biomolecular interactions with high sensitivity and label-free merit. SPR biosensors are being widely applied in basic biological, materials, health care, and other applications [1].

Conventional SPR sensing techniques are primarily based on intensity, angular, and spectral interrogation, respectively. The common drawback of these techniques is that they all suffer from limited detection resolution, which is around the order of merely 10^{-6} of the refractive index unit (RIU) [2]. Recently, measurement of SPR phase shift has been demonstrated for significant improvement in sensitivity. For example, a differential phase measurement employed in a Mach–Zehnder interferometer has been demonstrated with an achievement of 5.5×10^{-8} RIU [3]. It is noted, however, that the steep phase change occurs only in a small region within the plasmon resonance dip, where a limited dynamic range of 10^{-3}–10^{-4} RIU is found too narrow for practical applications. To optimize the dynamic range, several techniques have been demonstrated, including mixed interference signal detection technology [4] and the surface plasmon enhanced ellipsometry technique [5]. In these cases, however, the improvement in dynamic range was realized by trading in the sensitivity. Until recently, it was demonstrated that a detection resolution of 2.2×10^{-7} RIU and a dynamic range of 0.06 RIU have simultaneously been achieved by combining phase detection and angular interrogation [6]. These techniques are all based on differential phase measurement between p- and s-polarizations in an attenuated total reflection (ATR) configuration, which can be confined to only a fixed angle or a relatively small angular range. In this Letter, we propose a new scheme of phase-sensitive SPR (pSPR) for obtaining an ultra-wide dynamic range without sacrificing sensitivity. The proposed pSPR scheme is based on measuring the differential phase between radial and azimuthal polarizations in an inverted microscope. Since the signal beam focused by a total internal reflection fluorescence (TIRF) lens contains the entire angular range from 0 to the maximum angle of the lens, the dynamic range can further be improved compared with the ATR configuration. Moreover, with the technique of differential phase measurement between radial and azimuthal polarizations employed in our system, a very high sensitivity is obtained simultaneously.

It is known that linear polarized light contains both p- and s-polarizations naturally, leading to the wide application in differential phase measurement technology. In our scheme, as shown in Fig. 1, the differential phase measurement is implemented between two cylindrical

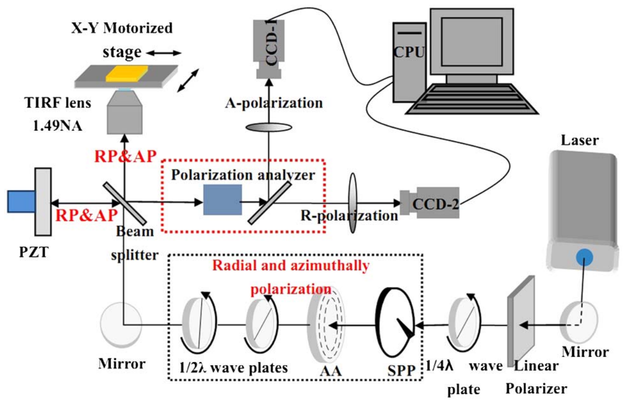

Fig. 1. (Color online) Experimental setup for measuring the differential phase between RP and AP beams in an inverted microscope configuration.

vector beams (CVBs), namely radially polarized (RP) and azimuthally polarized (AP) beams, with a number of good properties such as smallest focused spot ever experimentally demonstrated. A relatively simple technique comprising a microfabricated spiral phase plate and an azimuthal-type linear analyzer is applied to generate an AP beam. Details about the beam generation can be found in our previous work [7,8]. Following that is a polarization rotator consisting of two half-wave plates enabling switching between p-polarized and s-polarized light with respect to the interface. The angle between their axes is$\Delta\theta$, and the conversion process can mathematically be expressed by applying the rotation matrix $R_{\Delta\theta}$ to the two half-wave plates M_0. The combined action of both half-wave plates is

$$\begin{aligned} R_{\Delta\theta}\cdot M_0\cdot R_{-\Delta\theta}\cdot M_0 &= \begin{bmatrix} \cos(\Delta\theta) & -\sin(\Delta\theta) \\ \sin(\Delta\theta) & \cos(\Delta\theta) \end{bmatrix}\begin{bmatrix} -i & 0 \\ 0 & i \end{bmatrix} \\ &\times\begin{bmatrix} \cos(\Delta\theta) & \sin(\Delta\theta) \\ -\sin(\Delta\theta) & \cos(\Delta\theta) \end{bmatrix}\begin{bmatrix} -i & 0 \\ 0 & i \end{bmatrix} \\ &= \begin{bmatrix} -\cos(2\Delta\theta) & \sin(2\Delta\theta) \\ -\sin(2\Delta\theta) & -\cos(2\Delta\theta) \end{bmatrix} \\ &= -R_{2\Delta\theta}. \end{aligned} \tag{1}$$

The matrix $R_{2\Delta\theta}$ performs a simple "barrel" rotation of $2\Delta\theta$ at each point around the optical axis while preserving the polarization class of any input beams. After incidence of the AP beam to this polarization rotator, the emergent light E_{out} is

$$\begin{aligned} E_{\text{out}} &= -R_{2\Delta\theta}\cdot E_{\text{in}} \\ &= \begin{bmatrix} -\cos(2\Delta\theta) & \sin(2\Delta\theta) \\ -\sin(2\Delta\theta) & -\cos(2\Delta\theta) \end{bmatrix}\begin{bmatrix} -\sin(\theta) \\ \cos(\theta) \end{bmatrix} \\ &= \begin{bmatrix} \sin(2\Delta\theta+\theta) \\ -\cos(2\Delta\theta+\theta) \end{bmatrix}. \end{aligned} \tag{2}$$

When $\Delta\theta = 3\pi/8$, E_{out} is

$$E_{\text{out}} = \frac{\sqrt{2}}{2}\begin{bmatrix} -\sin(\theta) \\ \cos(\theta) \end{bmatrix} + \frac{\sqrt{2}}{2}\begin{bmatrix} \cos(\theta) \\ \sin(\theta) \end{bmatrix}, \tag{3}$$

containing half an RP and half an AP component, respectively. By adjusting the angle between the axes of two half-wave plates, a beam mixed with different RP and AP proportions is generated, as verified experimentally in Fig. 2. By increasing the angle from 45 to 90 deg for a pure RP and a pure AP beam, respectively, the intensity of the dark ring corresponding to the resonance angle [8] is decreased gradually until it completely disappeared. This is due to the fact that under a high NA focusing condition, the RP beam is completely TM polarized in all directions with respect to the surface being able to excite SP, while the AP beam is completely TE polarized without functionality for SP excitation. For a deeper theoretical understanding of producing SPs by a focused laser beam, interested readers are directed to [9–11].

Figure 1 demonstrates a schematic diagram of the experimental setup. In this scheme, a linear polarized

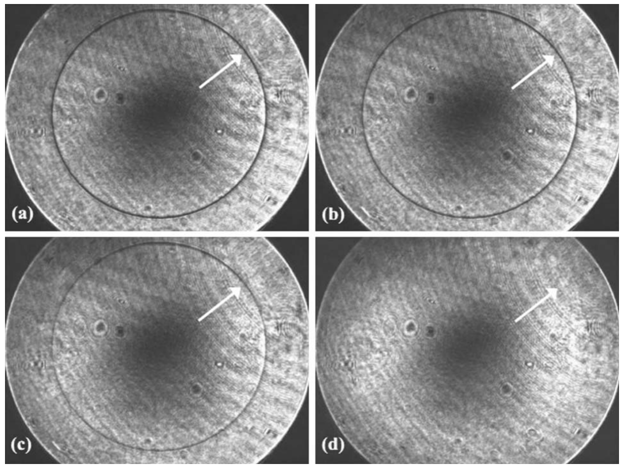

Fig. 2. Image captured on the CCD for different included angles between the two half-wave plates: (a) $\frac{\pi}{4}$, (b) $\frac{3\pi}{8}$, (c) $\frac{7\pi}{16}$, and (d) $\frac{\pi}{2}$. The inner dark ring corresponds to the SPR excitation angle.

780 nm laser source is used to generate the required half RP and half AP beam. Following that is a Michelson interferometer in which two interferometers (radial and azimuthal polarizations) are used in parallel. In the signal arm focused by the TIRF lens (Olympus $100\times$ NA 1.49), the RP beam (TM polarized) is modified by a surface plasmon wave after exciting SP; while the AP beam (TE polarized) is merely reflected by the metal–dielectric interface without disturbance. In the reference arm, both RP and AP beams are directly reflected by the reference mirror mounted on the end of a piezoelectric transducer (PZT) with a periodic linear phase shift. The phase changes of both radial and azimuthal polarizations at the SPR angle are measured simultaneously. The sensor surface is a 55 nm gold film, which is well optimized to provide a sharp jump of the phase of light reflected under SPR. In the output path, a polarization analyzer is used to separate the exit beam into RP and AP light. Two synchronized CCDs (1280×960 pixels) are used to capture the signal. Digitalized intensity data were then processed in a personal computer to deliver the differential phase information with a fringe analysis and phase extraction program.

Figure 3 shows the phase obtained at different pixels (corresponding to different incident angles) for different refractive indices (RIs). Here, the phase information comprises the averaged results of the phases of all of the pixels along the entire circular region associated with the SPR dip. It is seen that for each pixel, phase undergoes a sharp change for a narrow RI range, which is determined by optical properties of SPR. Moreover, with the shifting of pixel number, the corresponding most-sensitive RI range shifts progressively. This is due to the fact that for a given gold film thickness, the resonance angle where the most sensitive RI region locates increases with RIs of the samples. Thus by accumulating the maximum phase change from all pixels during a large RI change, the integrated sensor is able to carry out high sensitivity for a wide dynamic range. Furthermore, it is noted that the dynamic range is mainly determined by the angular range of the signal beam for a given gold film thickness. In our case, the signal beam focused by the

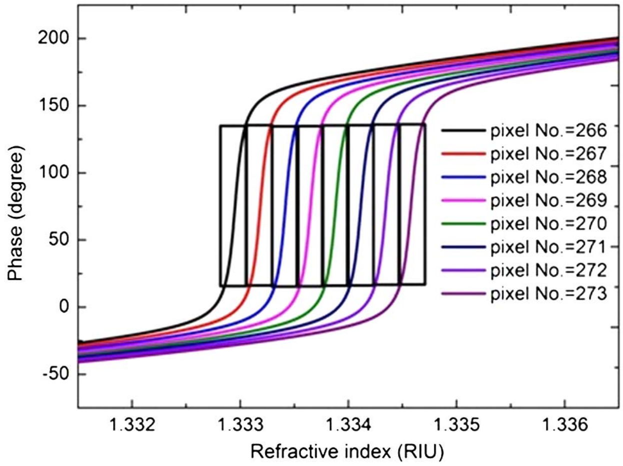

Fig. 3. (Color online) Phase changes versus refractive index at a series of pixels for 55 nm thick gold film.

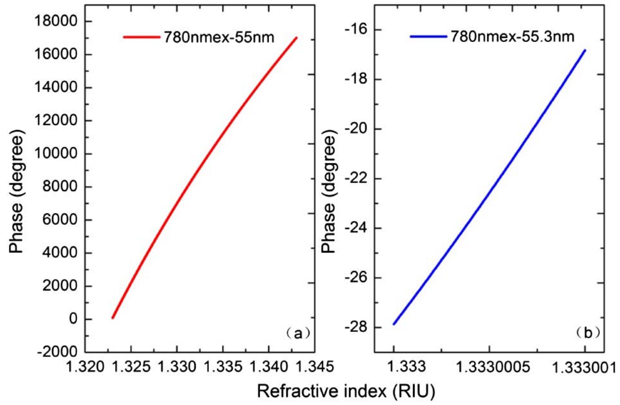

Fig. 4. (Color online) System response versus refractive index (a) from 1.320 to 1.340 RIU for a 55 nm thick gold film; (b) from 1.333 to 1.333001 RIU for a 55.3 nm thick gold film.

TIRF lens of 1.49 NA contains an extremely large angular range from 0 to 79.4 deg, which is normally impossible for an ATR configuration, resulting in an ultra-wide dynamic range from 1 to 1.4095 RIU [12].

To verify the ultra-wide dynamic range, we simulated the SPR differential phase response to a large range of RIs, and the result is shown in Fig. 4(a). It is clearly seen that this pSPR sensing system delivers a very high sensitive phase response up to 16935.84 deg at the ultra-large dynamic range of 0.02 RIU, indicating an averaged sensitivity threshold of 1.12×10^{-8} RIU (assuming 0.01° phase resolution).

The sensitivity limit of the proposed system is affected by several factors, such as thickness of the gold film and the RI detected. For a given thickness, the system delivers different phase response properties to different RIs, which can be seen from the nonlinear system response curve in Fig. 4(a). To obtain the sensitivity limit around 1.333 RI, which is the typical condition for most biological samples located in an aqueous medium, the gold film thickness is well optimized to 55.3 nm. The calculated sensitivity limit curve is shown in Fig. 4(b). We can see that the RI change from 1.333 to 1.333001 RIU within a phase change of 11.04 deg will result in sensitivity as high as $\pm 9.05 \times 10^{-8}$ RIU/1 deg. It is comparable to the best result reported.

In addition to SPR sensing, the proposed scanning microscopic system is able to implement SPR imaging with the help of an X–Y motorized stage as demonstrated in our previous work [8,13], where lateral imaging resolution is maintained by the focused virtual probe of the RP beam. The acquired data is visualized in the form of a local RI map revealing surface morphology at the cell–metal interface. However, the sensitivity is limited to the order of 10^{-4} RIU in the past. With the proposed technique, both high spatial resolution and ultra-high sensitivity can be integrated in a microscope for imaging as well as sensing. This offers great opportunities for highly sensitive visualization of local RI differences between highly resolved adjacent areas in biological samples.

This work was partially supported by the National Natural Science Foundation of China under grant nos. 10974101, 61036013, and 61138003. X.C.Y. acknowledges the support given by the Ministry of Science and Technology of China under grant no. 2009DFA52300 for China–Singapore collaborations, the National Research Foundation of Singapore under grant no. NRF-G-CRP 2007-01, and Tianjin Municipal Science and Technology Commission under grant no. 11JCZDJC15200.

†These authors contributed equally to this Letter.

References

1. R. L. Rich and D. G. Myszka, J. Mol. Recognit. **18**, 431 (2005).
2. Y. H. Huang, H. P. Ho, S. Y. Wu, and S. K. Kong, Adv. Opt. Technol. **2012**, 471957 (2012).
3. S. Y. Wu, H. P. Ho, W. C. Law, and C. L. Lin, Opt. Lett. **29**, 2378 (2004).
4. W. Yuan, H. P. Ho, Y. K. Suen, S. K. Kong, and C. Lin, Appl. Opt. **46**, 8068 (2007).
5. H. P. Ho, W. C. Law, S. Y. Wu, X. H. Liu, S. P. Wong, C. Lin, and S. K. Kong, Sens. Actuators B **114**, 80 (2006).
6. Y. H. Huang, H. P. Ho, S. Y. Wu, S. K. Kong, W. W. Wong, and P. Shum, Opt. Lett. **36**, 4092 (2011).
7. K. J. Moh, X. C. Yuan, J. Bu, D. K. Y. Low, and R. E. Burge, Appl. Phys. Lett. **89**, 251114 (2006).
8. K. J. Moh, X. C. Yuan, J. Bu, R. E. Burge, and B. Z. Gao, Appl. Opt. **46**, 7544 (2007).
9. H. Kano, S. Mizuguchi, and S. Kawata, J. Opt. Soc. Am. B **15**, 1381 (1998).
10. H. Kano and W. Knoll, Opt. Commun. **153**, 235 (1998).
11. H. Kano and W. Knoll, Opt. Commun. **182**, 11 (2000).
12. K. J. Moh, X.-C. Yuan, J. Bu, S. W. Zhu, and B. Z. Gao, Opt. Lett. **34**, 971 (2009).
13. K. J. Moh, X.-C. Yuan, J. Bu, S. W. Zhu, and B. Z. Gao, Opt. Express **16**, 20734 (2008).